A Study of the Peculiarities of Molding and Structure Formation of Compacted Multicomponent Silicide Composites

Article *in* Journal of Superhard Materials · June 2022

DOI: 10.3103/S1063457622030054

CITATIONS
5

READS
32

5 authors, including:

Serhiy Lytovchenko
V. N. Karazin Kharkiv National University
61 PUBLICATIONS **139** CITATIONS
SEE PROFILE

Edwin Gevorkyan
Ukrainian State University of Railway Transport
109 PUBLICATIONS **546** CITATIONS
SEE PROFILE

Liudmyla Voloshyna
Ukrainian State University of Railway Transport
17 PUBLICATIONS **23** CITATIONS
SEE PROFILE

ISSN 1063-4576, Journal of Superhard Materials, 2022, Vol. 44, No. 3, pp. 175–189. © Allerton Press, Inc., 2022.
Ukrainian Text © The Author(s), 2022, published in Nadtverdi Materialy, 2022, Vol. 44, No. 3, pp. 35–52.

PRODUCTION, STRUCTURE, PROPERTIES

A Study of the Peculiarities of Molding and Structure Formation of Compacted Multicomponent Silicide Composites

S. V. Lytovchenko[a], E. S. Gevorkyan[b, *], V. P. Nerubatskyi[b], V. O. Chyshkala[a], and L. V. Voloshyna[b]

[a] *Karazin Kharkiv National University, Kharkiv, Ukraine*

[b] *Ukrainian State University of Railway Transport, Kharkiv, Ukraine*

**e-mail: edsgev@gmail.com*

Received December 8, 2021; revised December 20, 2021; accepted December 20, 2021

Abstract—Technology for the preparation of carbide and multicomponent powders from scrap of hard alloys and tungsten anhydride for further use in the formation of eutectic coatings have been developed in the laboratory. The temperature–time parameters of a process for obtaining powders with the required chemical composition are determined. It is established that compositions with a controlled melting point in the range of 1000–1200°C can be obtained when boron and silicon additives are introduced into these powders in the quantitative ratios corresponding to eutectic compositions. Dross mixtures based on Ni–Si–B and Ni–Cr–Si–B composite powders with reinforcing additives from industrial and laboratory-synthesized refractory silicides and carbides are prepared. Eutectic coatings whose solid component has a microhardness of 18–26 GPa and plastic matrix has a microhardness of 11–15 GPa are prepared by melting dross mixtures on the substrates made of steel and molybdenum. The comparison of structural characteristics and properties of coatings shows that the high-speed melting allows one to obtain the required thickness of the protective layer and to prevent excessive embrittlement of the substrate due to the formation of boride phases. It is found that the addition of molybdenum disilicide in a concentration of up to 50 wt % increases the homogeneity of the coating without reducing its hardness. The coatings are characterized by high corrosion resistance at temperatures around 1000°C.

Keywords: silicide composite, consolidation, thermal conductivity, multicomponent powder, reinforcing additive, dross mixture, eutectic coating

DOI: 10.3103/S1063457622030054

INTRODUCTION

The powder metallurgy and powder materials science are among the promising areas of physical materials science, which provide the development for many advanced technologies [1]. The efforts toward improving known materials and developing new types of consolidated materials, which have practically moved to a new research field of ultra- and nanodispersed powder ingredients, are very relevant.

Along with high heat resistance, the ability to form products with complex shapes is an important property of refractory metal silicides in powder metallurgy. Naturally, it is necessary to optimize the processes of consolidation of fine powders and to control both technological characteristics and performance of final products in such studies [2, 3].

Currently, the main application area of materials based on refractory metal disilicides—primarily, molybdenum disilicide—is the manufacture of high-temperature heating elements for electric resistance furnaces, as well as crucibles, protective screens, covers, and other elements of high-temperature units and devices for various industries [4]. Products are obtained using various technologies of consolidation of powder raw materials [5, 6].

It should be borne in mind that most of the industrially developed technologies of compaction of silicides involve the introduction of special additives to improve the technological effectiveness of the consolidation process or provide the material with special properties [7, 8]. The content of these additives can be very complex [9, 10] and is nearly always the subject of know-how of the manufacturer, so their impact on the properties and structure of the material is very difficult to evaluate. As a result, data on the properties of consolidated silicide materials and promising results on improving them may differ substantially in studies of different authors.

The preparation of high-purity low-oxidized powders obtained by physical or chemical methods of synthesis in submicrometer and nanometer scales, the alloying and fusion of silicide powders with various additives, and the creation of reinforced composites are important problems in the development of new consolidated high-temperature silicide materials [11, 12].

EXPERIMENTAL

In the study of the consolidation processes of refractory metal disilicide powders, samples prepared from $MoSi_2$ and WSi_2 powders with a dispersion of 5–10 μm were studied. Consolidation was performed by vacuum sintering and hot vacuum pressing [13, 14]. To obtain samples with the maximum density scatter, the technological conditions of consolidation were varied in a fairly wide range.

Both free flowing powders and precompacted powders were subjected to sintering. The formation of bodies is among the principal operations in the production of powder products. During molding, the shape and size of the products and the basic properties of the material are determined.

Compaction (preliminary molding) of disilicide powders was performed on a hydraulic press in steel cylindrical molds with a diameter of 10–12 mm at room temperature and with overpressures of 30, 60, and 100 MPa (discrete cold process in air with relatively slow increase of unidirectional pressure).

After cold molding, the powder blanks have weak mechanical properties, so the pressed blanks were subjected to consolidation by sintering to ensure the required strength and provide other necessary physicochemical properties.

The process of sintering was carried out in vacuum in a SShVE unit at temperatures of 1100–1500°C. The duration of high-temperature exposure was 30–240 min. Free-flowing powders were sintered in graphite crucibles, and tablets of precompressed silicides were sintered on alumina substrates.

External geometric parameters of the samples were not rigidly fixed; the shrinkage during sintering was insignificant. For further research, sintered samples of a cylindrical shape with a height of 5–10 mm were selected.

Powder consolidation conditions and technology determine the structural and phase state of the obtained materials and their properties. For high-temperature applications of silicides obtained by powder technology, it is very important to establish relationships between structural parameters, such as density and porosity, and thermal properties (primarily with thermal conductivity). The density and apparent porosity of the samples were calculated on the basis of measurements of the geometric sizes of cylindrical samples (their diameter and height) and their actual weight. The weight of the samples was determined by weighing on laboratory scales with an accuracy of 0.01 g; during the calculation, the weight of air in the pores of the samples was neglected. Specific measured and calculated values are given in Table 1.

As a result of consolidation, samples with a density of up to 6.2 (for $MoSi_2$) and 7.81 (for WSi_2) g/cm^3 were obtained, which agrees well with published data on the theoretical and experimental density. The porosity of the samples of $MoSi_2$ and WSi_2 varied from 60 to <1% and from 74 to 15%, respectively.

The theory cannot accurately predict the thermal conductivities of specific substances, so the only option for determining the value of thermal conductivity with the required reliability is an experimental study [15]. In general, the thermal conductivity is a function of the structure, density, humidity, pressure, and temperature, i.e., the condtitions under which the test substance is placed.

The basis of most methods for determining the thermal conductivity of solids is a theoretical analysis of steady-state one-dimensional thermal and temperature fields in samples [16, 17]. This approach is applied to samples with plate-like (flat half-space) or cylinder-like (cylindrical half-space) shapes. A number of special devices [18, 19] with a common control measuring and computing integrated unit have been developed for standard thermal conductivity measurements; for example, an A-3M high-temperature device covers the thermal conductivity range from 5 to 20 W/(m °C) and operates in the range from room temperature to 800°C, which is insufficient for such high-temperature materials as silicides of refractory metals.

Studies of the thermal conductivity of disilicide samples were performed on a special device placed in the vacuum chamber of a GDP-5M universal station. The steady-state heat flux method was used to measure the effective thermal conductivity [20, 21]. The scheme of measurements is given in Fig. 1.

Heat flow meter *2* and sample *3* were placed between heat source *1* and heat sink radiator *4*. The measuring column composed of three cylinders with a diameter of 15 mm and a height of 17 mm each, which were soldered at the bases and made of steel 12Kh18N9, was used as a heat flow meter. An increase in the thermal conductivity of this steel in the temperature range from room temperature to 1400°C follows an

Table 1. Thermal conductivity and properties of disilicide samples

Silicide	T_{sint}, °C	p_{mold}, MPa	λ, arb. unit at T (°C)				d, mm	h, mm	ρ, g/cm^3	Porosity, %
			25	100	250	550				
$MoSi_2$	1100	0	Unsintered powder							
		30	0.58	0.72	0.97	1.48	11.7	2	3.72	49
		60	0.90	1.12	1.69	2.22	12	2.8	4.42	27
	1300	0	Unsintered powder							
		30	0.68	0.87	1.09	1.56	12	2	3.98	35
		60	0.82	0.95	1.68	2.13	12	3	4.12	32
	1500	0	0.50	0.68	0.95	1.28	11.9	8.8	2.45	60
		30	1.48	1.52	1.98	2.68	11.4	3.5	5.32	13
		100	3.16	3.67	4.51	4.98	11.2	5.4	6.00	2
	1350 (HP)	40	3.44	3.95	4.73	5.33	12	5.2	6.2	<1
WSi_2	900	0–100	Unsintered powder							
	1100	0	Unsintered powder							
		30	0.89	0.97	1.52	1.77	12.2	2.8	5.5	37
		60	1.03	1.04	1.80	2.25	12	3.9	6.25	29
	1300	0	0.63	0.76	1.24	1.58	11	4.2	2.48	74
		30	0.94	1.08	1.64	2.07	12.7	2.7	5.7	33
		60	1.08	1.12	1.96	2.41	12	3.2	6.35	26
	1500	0	0.63	0.81	1.37	1.62	11.5	5.7	2.2	71
		30	0.94	1.08	1.75	2.23	12.1	3.8	5.96	31
		100	2.94	3.24	3.84	5.04	11.8	5.9	6.37	22
	1350 (HP)	40	4.28	5.63	7.03	8.84	12	5.1	7.81	15

T_{sint} is the sintering temperature; HP stands for samples obtained by hot pressing; p_{mold} is the excess pressure during molding ($p_{mold} = 0$ corresponds to bulk powders).

almost linear pattern. The thermal conductivity ranges from about 12 to 28 W/(m °C), which facilitates the measurement of small heat fluxes flowing through the measuring cell.

The cylinder bases of the measuring column were in thermal contact with the heat source (upper bases) and the sample (lower base). Accordingly, the upper base of the sample was in thermal contact with the

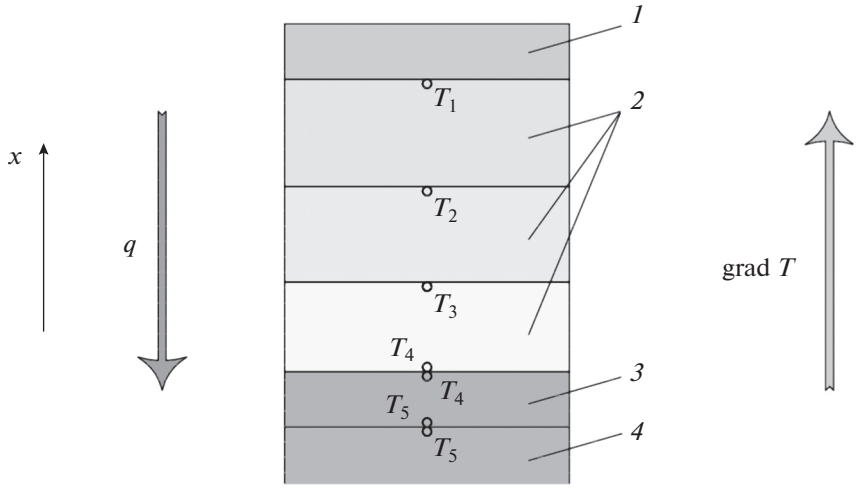

Fig. 1. Schematic representation of the measuring cell.

lower base of the measuring column, and the lower base of the sample with the surface of the heat exchanger. The required thermal contact was achieved using a special clamping device.

To minimize heat losses due to heat dissipation into the environment, the measuring cell was placed in a multilayer reflective container made of molybdenum and tungsten foil inside a chamber of a VUP-5M device. Measurements were performed under a vacuum pressure below 10^{-3} Pa.

To measure the temperature of the corresponding surfaces, tungsten–rhenium thermocouples were installed at the column junctions (T_2 and T_3), at the points of contact with the heater (T_1) and the sample (T_4), and at the point of contact of the sample with the radiator (T_5). Additional thermocouples T_6 and T_7 controlled the temperature of the clamping device.

In the calculations, the contact surface between the specimen under test and the measuring column is taken as a starting point for the x coordinate. In this geometry, the heat transfer surface is located at point $x = 5.1$ cm, and the heat sink surface is at point $x = -h$ cm, where h is the height (in cm) of the cylindrical sample (tablet thickness).

The steady heat flow through the heat flow meter from the electric heater was fed to the test sample and then removed from it by a radiator, i.e., the heat sink exchanger whose role was played by a water-cooled copper cylinder.

The measured temperature distribution at points T_1–T_5, the temperature difference on the sample at T_4–T_5, predetermined thermal conductivity κ_c of contacts of the sample with the measuring column and radiator [22], and the value of effective thermal conductivity λ_1 of the material of the measuring column were used to calculate effective thermal conductivity λ_2 of the material under test.

Using Fourier's law, the heat flow through a heat flow meter can be expressed as follows:

$$q_1 = -\lambda \frac{\Delta R}{\Delta x}, \tag{1}$$

where q_1 is the heat flow through the measuring column in the region between points T_1 and T_3, λ_1 is the thermal conductivity coefficient of the material of the measuring column, and $\Delta T/\Delta x$ is the temperature gradient along the meter in the region between points T_1 and T_3.

The expression for heat flow q_2 through the contact surface of test sample *3* with heat flow meter *2* (see Fig. 1) has the following form:

$$q_2 = -\kappa_c \left(T_4 - T_4' \right), \tag{2}$$

where κ_c is the thermal conductivity of the contact between surfaces of the sample and the measuring column, T_4 is the column temperature right above the contact surface, and T_4' is the temperature of the sample right below the contact surface.

Heat flow q_3 through the test sample is

$$q_3 = -\lambda_2 \frac{\left(T_4' - T_5' \right)}{h}, \tag{3}$$

where T_4' is the temperature of the sample right below the contact surface between the sample and the heat flow meter; T_5' is the temperature of the sample right above the contact surface of the sample, i.e., the heat sink exchanger; λ_2 is the effective thermal conductivity of the sample; h is the height of the sample.

Heat flow q_4 through the contact surface of the sample and the heat sink exchanger is equal to

$$q_4 = -\kappa_h \left(T_4' - T \right), \tag{4}$$

where κ_h is the conductivity of the surface contact between the sample and heat sink exchanger, T_5 is temperature of the radiator right below the contact surface, and T_5' is the temperature of the sample right above the contact surface.

If we consider the process to be steady and neglect heat loss through to the environment and structural elements of the measuring cell, then the equality of all heat flows must be observed, i.e.,

$$q_1 = q_2 = q_3 = q_4. \tag{5}$$

By excluding unknown values of T_5' and T_4' from the equations, we obtain the following expression for the effective thermal conductivity of the sample:

$$\lambda_2 = \frac{\left(\lambda_1 h \frac{\Delta T}{\Delta x}\right)}{(T_4 - T_5) - \left(2\lambda_1 \frac{\Delta T}{\Delta x \kappa_c}\right)}. \quad (6)$$

Mean temperature gradient $\Delta T/\Delta x$ in the measuring column used in this expression was calculated by the method of least squares from the values of temperature at points T_1, T_2, and T_3, and the distances between these points; the averaging was performed for five separate measurements. On the basis of the same data, five arithmetic mean values of the temperature of the measuring column were calculated and then averaged over five groups of data. The obtained value of T was used to calculate thermal conductivity λ_1 of the heat flow meter. A similar method was used to determine mean temperature difference between points T_4-T_5, which was used to determine the effective thermal conductivity of the sample and the mean temperature of the sample.

The thermal conductivity of the 12Kh18N9 steel was determined according to [23]. Thermal conductivity κ_c of the contacts of the sample was determined by precalibration.

It should be noted that the used methodology and reference data do not allow one to determine the absolute values of thermal conductivity in standard physical units. The values obtained in some conventional units ultimately lead to adequate qualitative estimates of the temperature dependence of the thermal conductivity of silicides [24].

Consolidation of the samples by hot pressing or vacuum sintering made it possible to vary the density and porosity of the products in a wide range (between values differing by a factor of 30). With a porosity of more than 10%, the thermal conductivity of the samples is relatively small and depends little on the porosity value. A noticeable increase in the thermal conductivity was observed in dense samples with a porosity of 1–3%.

Temperatures in the range of 1300–1500°C are acceptable for sintering. Smaller temperature values do not allow one to gain the required properties. Higher temperature is impractical, only worsens the energy consumption of the process rather than lead to a noticeable change in the density.

There is some increase in the thermal conductivity with an increase in the temperature of sintering of the samples, but no specific quantitative estimates were possible. The observed increase can be explained by structural changes in the samples, namely: the higher sintering temperature increases the contact area of individual powder particles and accelerates diffusion, which strengthens the bonding between particles and promotes heat transfer.

With the same porosity of the samples obtained by sintering and hot pressing, the thermal conductivity achieved with hot pressing is higher. This result is quite predictable; it only confirms the well known data on the positive effect of hot pressing on the mechanical properties of the material. Comparison of data on the porosity and thermal conductivity confirms the logical conclusion that the porosity is a determining factor in the final value of thermal conductivity.

Practice shows that the use of multiphase and multicomponent coatings, which can often be considered as an independent composite unit, is an acceptable and often the best option for protection against multifactorial destructive effects [25, 26]. Varying the composition of the coating makes it possible to adjust its properties without substantially changing the overall functionality of the material. This approach meets the modern requirements for a critical attitude toward the universality of functional materials and strengthening the role of specialized technical solutions aimed at achieving the best results under specific operating conditions [27, 28].

If products operate under conditions of high-temperature corrosion and abrasive wear with variable load, then composite materials in which the solid reinforcing phase is placed in a plastic matrix show the best performance. Eutectic-type alloys capable of providing temperature stability of metal-coating systems up to a temperature of 0.9 eutectic melting point are an important class of refractory materials for the formation of wear-, corrosion-, and heat-resistant functional coatings [29, 30]. Improvements in the structure and properties of coatings are achieved by creating a heterogeneous dispersed/ordered or fairly homogeneous amorphous/crystalline structure.

Although chemical heat treatment (CHT) is the simplest and most common technology for forming functional coatings, this technique often requires quite high temperatures, and is time and energy con-

suming. It should be noted that prolonged thermal exposure can lead to a substantial change in the mechanical properties of the substrate due to recrystallization and diffusion processes.

These drawbacks can be overcome to some extent by using compositions that form relatively low-melting eutectic alloys. The process of coating formation can be enhanced by increasing the rate of diffusion of saturating elements in the liquid eutectic layer formed when the components of the saturating mixture come into contact with the surface of the material to be protected. Quite a lot of studies have been devoted to studying the formation of various coatings of eutectic compositions [31, 32]. The coatings of Ni–Cr–Si–B compositions that sometimes contain solid additives are among the most actively studied multicomponent silicon-containing coatings [33, 34].

Reinforcing additives of industrially manufactured molybdenum and titanium disilicides, and WC and WC–Co carbide materials obtained independently in laboratory conditions were used to create technologies for the formation of multiphase composite coatings.

The disposal of scrap and waste of hard alloys and their processing into powders of the WC–Co or WC–Ni composites with the needed composition and dispersion is an option for obtaining carbide additives for their further use in the formation of composite coatings [35].

According to the traditional technology of production of WC–C carbide compositions, a mixture of polyhedral WC and C powders (particle size about 1 μm) is pressed and sintered or subjected to hot pressing. The sintering is carried out at a temperature of about 1400°C. This temperature is higher than the melting temperature of the eutectic between WC and Co, and a liquid phase is formed during processing. Complex changes occur in the process of annealing, but a simplified version of the process provides an adequate model to explain the final microstructure [36]. During sintering, tungsten carbide diffuses into solid cobalt, which turns into liquid at a content of about 30% WC[1]. The liquid is able to wet the remaining WC particles until reaching equilibrium (at 50% WC). The volume of components is greatly reduced during sintering. Moreover, recrystallization and an increase in the size of WC particles occur. During cooling, the liquid phase release carbide particles and completely solidifies at a temperature of about 1320°C in accordance with the eutectic reaction. Further release of carbides was observed in the solid state until reaching the room temperature, at which WC is barely soluble in cobalt.

In large-scale industrial production, various processing schemes for scrap hard alloys have been implemented. The vast majority of them is based on the chemical dissolution of the hard alloy, the release of tungstic acid H_2WO_4 and cobalt oxides, subsequent reduction of tungsten and cobalt with hydrogen, and repeated high-temperature synthesis of WC. All chemical methods are associated with environmentally friendly production and considerable costs of washing sludge from impurities. The described technologies are acceptable in large-scale production of products from hard alloy with stable mass demand, but less expensive technologies are required for small-scale production of a wide range of products. Direct grinding of hard alloys by crushing in different mills leads to substantial wear of expensive components, and the resulting powder does not provide the required quality of products because of impurities and structural changes. Direct dispersion of the WC–Co carbide eutectic composite is inefficient due to the high strength and adhesion of the reinforcing phase in the case of sufficient viscosity and ductility of the matrix.

To strengthen the composite, the following technological scheme was implemented:

— preliminary embrittlement of the carbide material in the case of single or multiple pulsed vacuum annealing ($T \approx 1600$°C);

— dissolution of the cobalt matrix with zinc;

— removal of zinc;

— grinding of the synthesized material.

Cobalt is easily soluble in molten metals, such as iron and refractory metals. The choice of zinc as a solvent is connected with its availability, low melting (419° C) and boiling (906°C) points, rapid evaporation during heating in vacuum, and the simplicity of the distillation process.

It should be noted that zinc is easily distilled off at temperatures when cobalt is not sublimed, quite resistant to oxidation (especially in vacuum and inert atmosphere), and does not form strong compounds with crucible material and cobalt at temperatures above 900°C. The possibility of combining dissolution and distillation processes in one plant and the absence of reactions of zinc with hydrogen and carbon monoxide in the case of reduction of oxides and oxycarbides of cobalt and tungsten were taken into account.

[1] Hereinafter, the content of the components is indicated in wt %.

Table 2. Chemical compositions of the crude and synthesized materials

No.	Material	Content, wt %		
		WC	Co	Zn
1	Initial VK8	92.0	8.0	–
2	VK8–Zn alloy	46.1	4.1	49.7
3	Alloy after vaporization for 1 h at 1050°C	87.7	6.11	6.17
4	Alloy after vaporization for 3 h at 1050°C	92.0	7.95	0.01
5	Condensate of Zn vaporized for 3 h at 1050°C	–	0.01	99.9

The scrap of hard alloy VK8 was precrushed, grinded, mixed with granular zinc in the required proportions, and poured into a crucible made of graphite MPG-7. Zinc that was preliminarily distilled one time at 460°C to remove inclusions and oxides was used to dissolve the hard alloys. The crucible was placed in a SShV vacuum oven and closed with a graphite beaker so that the lid of the beaker was in the cold zone under the cooled upper flange of the vacuum unit. The capacitor was made of molybdenum sheet or graphite.

The chamber was filled with technical argon to atmospheric pressure and annealed. To increase the dissolution rate, the process should be carried out in the liquid phase, so the zinc content should be sufficiently high. The maximum allowable dissolution temperature is limited by the boiling point of zinc. With this purpose, a temperature range of 700–850°C and a component ratio of approximately 90% Zn–10% Co were chosen for the dissolution process on the basis of the Co–Zn phase diagram. For the initial scrap of hard alloys with the 92% WC–8% Co (alloy VK8), this roughly corresponds to a mixture of 50% VK8–50% Zn. The insolubility of tungsten and tungsten carbide in liquid zinc and the fact that no substantial distillation of zinc should occur in the process of dissolution were taken into account when choosing the ratio of components.

An increase in the dissolution temperature causes an increase in the pressure of argon in the chamber to 1.22×10^5 Pa. The measurements showed that no more than 10% of the initial amount of zinc evaporates in 1–3 h at temperatures of 800–880°C under such a pressure, so its content in the alloy was not corrected.

The kinetics of dissolution was monitored using the method of metallography (MIM-8) by measuring the thickness of the unreacted hard alloy layer. Experiments have shown that the reaction penetrates to a depth of 6–9 mm at temperatures of 700–800°C for 90 min and to a depth of 20 mm at 850°C. Thus, it was found that the time of complete dissolution of the matrix metal does not exceed the above time interval (1–3 h) in the case of preliminary crushing of carbide waste to pieces with a size of 1–3 cm.

After completion of the stage of high-temperature dissolution of the matrix metal, the chamber was evacuated and then the procedure of distillation and condensation of zinc was performed. The process is activated at temperatures of 800–880°C, at which intensive evaporation begins and then is inhibited. This fact is explained by the uneven content of cobalt and zinc on the surface and in the depth of WC–Co–Zn alloy samples. If the cobalt content in the alloy exceeds 30%, then the composition crystallizes and the diffusion rate of Zn to the distillation surface sharply decreases.

If these temperatures are used, then the distillation of zinc from the WC–Co–Zn alloy with a layer thickness around 20–30 mm is completed in 50–150 h. To accelerate the distillation, it is advisable to conduct the process at temperatures above the boiling point of zinc. Experiments have shown that all zinc is distilled off from the alloy in 1–3 h at temperatures of 950–1050°C, after which a loose porous product remains in the crucible, the volume of which is three times larger than the volume of the initial load of the hard alloy. The final dispersing of the powder was performed in a vibrating mill with a polyurethane container and corundum grinding bodies.

To optimize the temperature and time parameters of processing at different stages of the technological process and after its completion, X-ray fluorescence and chemical analyses of materials were performed (Table 2). Uncontrolled impurities (less than 0.1%) are not specified.

The obtained results show that the selected process parameters (line 4 in Table 2) allow one to obtain a powder of the required chemical composition and to condense almost pure zinc for further utilization.

The optimized process of direct processing of tungsten anhydride into a fine powder of tungsten monocarbide in vacuum is another technology used.

The main source material in the production of tungsten carbide and hard alloys based on it is tungsten trioxide WO_3. In large-scale industrial production, tungsten trioxide is most often reduced with hydrogen to metal, and then tungsten carbide is obtained by heating in a mixture with carbon black. The main problem with this technology is to obtain the content of bound carbon in an amount close to the theoretical value. At the same time, the content of free carbon, oxygen, and nitrogen should be kept as low as possible. Optimal technical composition of tungsten carbide contains 6.1–6.15% of carbon (including 0.05–0.1% of free carbon) required for the binding of impurities, primarily oxygen, which gets into the charge at different stages of the technological process.

Direct production of tungsten carbide from mixtures of tungsten trioxide and carbon is much less commonly used. This method is not widely used in industrial applications despite its undeniable advantages, such as being a single-step process, increased safety due to the use of anhydrous equipment, a low temperature of the process, and the fine dispersity of the product.

Tungsten trioxide and calcined carbon black or graphite are used for the synthesis of carbide at a ratio of 5.37 : 1, i.e., about 90% of the theoretical amount of carbon corresponding to reaction $WO_3 + 4C = WC + 3CO$, because the carbon monoxide formed in the reaction is involved in further carburization reactions.

The components of the charge were mixed using an aqueous solution of polyvinyl alcohol, because the components are poorly mixed in dry form in view of the large difference in density. The charge was placed in a graphite container and annealed in vacuum at a pressure of about 10^{-2} Pa with activation of the mixture during synthesis. The activation can be achieved by mechanical stirring or using vacuum plasma processes.

Reduction of tungsten trioxide with carbon begins at a temperature of 650°C, but a product free of oxygen is obtained only at a temperature of 1500°C. Experiments on the synthesis of tungsten monocarbide have shown that it is acceptable stepwise annealing in the following modes:

— heating with any rate up to 1050°C;

— exposure to a temperature of 1050–1100°C for 1 h;

— heating to a temperature of 1500°C with a rate of up to 0.5–0.8 °C/s;

— exposure to this temperature for up to 5 min;

— cooling together with the oven after the power is turned off.

As a result, tungsten carbide powder with a particle size of 0.5–15 μm was obtained. An X-ray diffraction analysis of the obtained powder showed the presence of traces of lower carbide W_2C in addition to tungsten monocarbide, which indicated incompletion of the reduction process. If the proportion of carbon ingredients in the mixture was increased by 5%, then no lower carbide W_2C was identified in the final product.

The developed technological process was optimized using the results of mass spectrometric analysis of the gaseous medium in the working chamber during the synthesis [37]. To collect gas samples at different stages of the process, an MX-7304 monopole mass spectrometer with an autonomous pumping system was connected to the working chamber of an SShV-1.2,5/25I2 vacuum station.

Under the conditions of high-temperature reactions with concentration changes, controlled components of the gaseous medium (CO^+, CO_2^+, N_2^+, C^+, O^+, O_2^+, and H_2O^+) were selected, after which the ionic current intensities of these characteristic components were continuously measured. The end of the synthesis process was determined at the time when the current intensities of all controlled substances went to a minimum level. Mass spectrometric control of the composition of the gaseous medium during the synthesis of tungsten carbide showed that the selected modes were close to optimal ones. The proposed method of diagnostics allows one to adjust the parameters of the technological process during its implementation in each separate case. Thus, it is possible to create an automatic control system for this process on the basis of an automated mass spectrometric complex, which will optimize energy consumption and appreciably bring the composition of the reaction products to the required substances.

A preliminary study of the process conditions and composition for the synthesis of tungsten carbide was performed with sample weights of up to 10 g.

After testing the conditions, the laboratory synthesis of tungsten carbide was carried out in an SShV vacuum unit with a working chamber with a diameter of 100 mm and a length of 300 mm. The graphite crucible had an inner diameter of 75 mm and a length of 250 mm. The initial portion of the charge con-

tained 100 g of WO_3 and 18.6 g of carbon black. The processing gave 106 g of tungsten carbide, which agrees well with theoretical calculations.

The maximum load of this crucible is 3.5 kg. In this case, the required power of the furnace is 8.5 kW. The time of the complete cycle of tungsten carbide production is 4.5 h, of which direct synthesis takes 1.5 h and the heating–cooling cycle takes 3 h. The process can be shortened by using pass-through furnaces with lockchambers for introducing and removing crucibles from the workspace.

The basic composition containing nickel, boron, and silicon (sometimes with chromium addition) was chosen as a base for composite metal–ceramic coatings. Carbide, hard alloy, and molybdenum disilicide powders were used as additional reinforcing additives.

The starting materials for the slurry were electrolytic nickel PNE-1 (purity 99.9%); polycrystalline silicon of the KPS-3 brand (99.9%), amorphous boron (99.8%), and chromium electrolytic scaly ERC-1 (99.9%). If necessary, the ingredients were further ground in a vibromill, after which a fraction with a dispersion of 10–20 μm was separated for further use. The prepared initial powders taken in the amount necessary to obtain the desired composition were mixed in a rotating mixer.

In addition to these materials, industrial powders ready for use of the PG-CP4 brand on a nickel base with 16.5% chromium, 3.7% silicon, 3% boron, and 0.8% carbon were used.

Self-manufactured tungsten carbide powders, powders of hard alloys VK6 and VK8 with a dispersion of 20–500 μm, and industrially produced powders of molybdenum disilicide with a dispersion of 40 were used as reinforcing additives.

Slurry compositions were prepared by mixing the powder components with a 0.5% aqueous solution of carbomethylcellulose.

To elaborate the technology of coating formation, sheet grade stainless steel of the Kh18N10T brand (overall size of the samples $40 \times 20 \times 1.5$ mm^3) and molybdenum foil of the MCh brand ($40 \times 20 \times 0.2$ mm^3) were used as substrate materials. The flat region of the slurry coating in the middle part of the samples was 15×15 mm^2 in size. The slurry was applied by single or multiple staining with a brush and subsequent drying; the total thickness of the dried layer of the slurry ranged from 0.5 to 2 mm.

The process of melting of the coating was conducted in two different ways. The first method is melting under a vacuum pressure of 10^{-3}–10^{-2} Pa in the working chamber of a modernized SShV unit. The samples were mounted in water-cooled current leads and heated by direct electric current until the coating melts. The temperature of the high-temperature zone was controlled by a VR5/20 thermocouple. The appearance of the melt was detected visually through an inspection window in the upper lid of the vacuum chamber. The standard thermal exposure method included heating until reaching the melting point (about 10 s), short-term (2–4 s) eequilibration in the liquid phase, and cooling to ambient temperatures (about 30 s).

According to the second method, the coating was melted on the stand for electrospark butt welding by ultrashort electropulse heating in air. In this treatment, the liquid phase in the coating exists for a few tenths of a second. The size of the melting region is limited by the size of the contact surface of the electrodes, which had a diameter of 5 mm.

The structure of the obtained materials with eutectic coatings was examined by electron (a JSM-7001F instrument) and optical (a MIM-8 instrument) microscopy; the mechanical properties were characterized by determining microhardness $H\mu$ and hardness HV.

RESULTS AND DISCUSSION

The Ni–Ni_3B eutectic alloy with a melting point of 1091°C served as a basis for the obtained coatings of the Ni–B system, and the addition of silicon and chromium primarily provided the lowering of the melting temperature of the composition. Accurate determination of the melting temperature of the coating was largely complicated by the variability of its composition depending on the composition of a particular substrate and by the peculiarities of the melting and crystallization conditions, which may markedly differ from the equilibrium conditions.

It should be noted that the slurry method used to obtain the coating is, on the one hand, easy to implement and affordable, and on the other hand, one of the main causes of instability of the coating under prolonged high temperature operation and high mechanical loads. In addition, the possible phase transformations leading to phase influx in the matrix component make it difficult to create high-quality coatings.

Studies have shown that the structure of the coating slightly depends on the material of the used substrates (steel and molybdenum) and is mainly determined by the composition of the slurry and the thermal

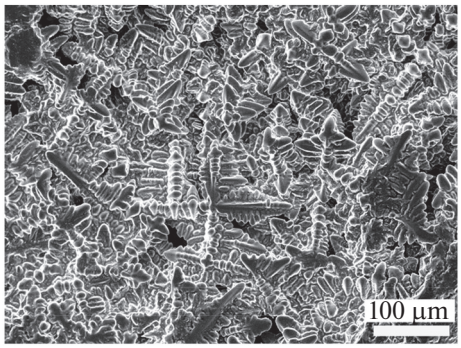

Fig. 2. Microstructure of the Ni–Si–B coating melted at temperatures of 1020–1040°C.

parameters for melting. Some differences were observed in the boundary regions that are in contact with the coated substrate. These differences are related to the different electrophysical and thermal properties of substrates (electrical resistance, thermal conductivity, heat capacity, and wettability) and, to a lesser extent, with the formation of various chemical compounds in the boundary layer.

The heating of the molybdenum sample with ternary coating Ni–5% B–5% Si to a temperature of 800°C activates the exothermic reaction of formation of silicides and nickel borides, the occurrence of which was detected visually. Mechanical stresses in the coating–substrate system lead to cracking of the slurry layer, and the exothermic reaction results in an additional local increase in the temperature, which leads to the formation of a liquid eutectic phase, initially in the hottest regions near the substrate with the slurry. The liquid easily penetrartes through the defects of the slurry layer onto the surface, where it crystallizes upon cooling.

The metallographic and X-ray diffraction analyses showed that the basis of the coating is a 96.36% Ni + 3.64% B eutectic mixture formed between nickel and its lower boride Ni_3B. Given that boron is an active reducing agent for oxides, which can be present as technological impurities in the coating, some excess of it in the original powder with respect to the eutectic composition is completely proper and even necessary. The Ni–Ni_3B eutectic ensures good spreading of the melt and wetting of the substrate surface, which determines the high adhesion of the coating.

On the other hand, the surface of the unmelted slurry wets much worse (the contact angle is greater than 110°) and the eutectic gather on the surface as individual spheroidal droplets when it crystallizes after melting to this stage (after heating for 3–4 s). At temperatures of 1020–1040°C, the slurry coating is rapidly melted and a conventional dendritic structure is formed during the crystallization stage (Fig. 2).

Dendritic components are formed in coatings with a thickness of growth layers from 50 to 300 nm. It should be noted that the resulting coating is quite compact, and its porosity is negligible and does not exceed 2% according to estimation. The fluidity of the coating substantially depends on the shape of the liquidus curve of the Ni–B eutectic. In pre-eutectic compositions, the liquidus line rises sharply when the boron content decreases; the melting temperature of the composition increases by about 100°C for each weight percent of reducing the boron content, so rather small temperature fluctuations during melting of the coating relatively weakly change solid and liquid phases and have a small effect on the motility moveability of the coating. In supereutectic compositions, whose phase diagrams have a sloping liquidus line (the temperature increases by about 25°C when the boron content increases by 1%), even a slight overheating is accompanied by a sharp increase in the liquid phase volume and, accordingly, moveability of the melt.

Additions of silicon to the Ni–B system lead to a slight decrease in the temperature of the eutectic, which is represented by a complex set of nickel silicoborides and double phases [38].

Rapid cooling of the molten cermet coating leads to considerable concentration of internal stresses in the coating, the relaxation of which initiates the cracking of large crystallites of flaky borides under loads below the yield point of the matrix, which is usually characteristic of cast materials.

Dependent on the conditions of cooling, the microhardness (with an indenter load of 50 g) of a nickel-based solid solution is 400–450 kgf/mm^2; the microhardness of a solid solution of boron in nickel is about 190 kgf/ mm^2 in the case of pure eutectic and 1100–1500 kgf/mm^2 in the case of complex eutectics. Hardness *HV* of the Ni–Si–B triple eutectic is close to 900 kgf/mm^2.

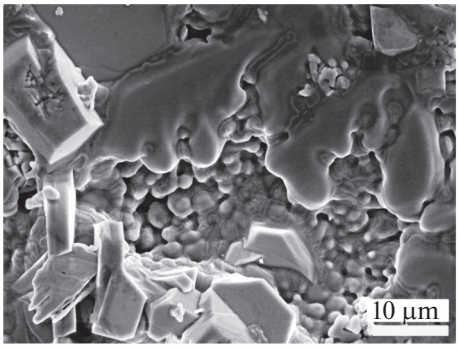

Fig. 3. Beginning of melting of the Ni–Cr–Si–B coating with additives (T = 1050°C).

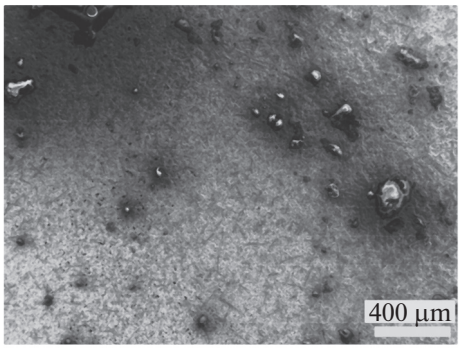

Fig. 4. Surface of the coating melted from the PG-CR4 and VK6 powders at a temperature of 1080°C.

In the process of coating preparation, intermediate layers of solid solutions that reduce the gradient of properties and stresses between the coating and the substrate were naturally formed. It was found that boron (which has a small ionic radius) diffuses rapidly into the substrate and compacts it. At the same time, it substantially increases the fragility of the coating. Additions of chromium and silicon reduce this negative effect of the presence of boron.

Slurries based on the standard industrial powder of the PG-SR4 brand (Ni–Cr–Si–B) and powders of hard alloys VK6 and VK8 (up to 50% in the composition of a slurry powder) melt at a slightly higher temperature. In the initial stage of melting, crystals of the disintegrated hard alloy and molten eutectic alloy were observed in the structure (Fig. 3). This stage can be considered as a combination of melting and sintering, which leads to the formation of primary mechanical contacts between the constituent substances of the composite. Good wetting and interaction were observed at the points of contact of the eutectic matrix of the composite with the reinforcing particles of the hard alloy.

A temperature of about 1080°C is required for complete melting of the Ni–Cr–Si–B/WC–Co composite slurry. The presence of island areas of borosilicate glass with sizes from tens to hundreds of micrometers is a characteristic structural feature of the coating surface (Fig. 4). The hardness of the pure Ni–Cr–Si–B eutectic is 800–900 kgf/mm^2, and the hardness of the dispersion of reinforcing inclusions in it is 1100–1200 kgf/mm^2.

Microstructural Studies of the steel coating revealed the presence of individual elongated pores that are mainly located around the reinforcing carbide inclusions.

Boron diffuses into the base along the grain boundaries to a depth of 20 μm, but the formation of a substantial amount of intermediate phases of brittle iron boride at the boundary between the base and the coating is not detected. Their absence can be explained by the short duration of the melt. This suggests that the embrittlement of coated samples in the case of melting for 2–4 s will be insignificant.

The slurry Ni–Cr–Si–B/WC–Co coating on steel was melted, in addition, by electropulse heating in air. The duration of the maximum thermal exposure on the object in this process was reduced to a few tenths of a second, due to which there is no significant oxidation of the materials. A eutectic compostition

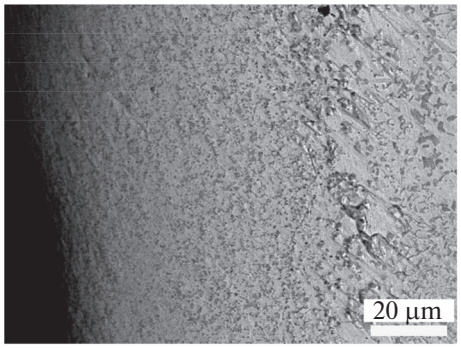

Fig. 5. Surface of the coating melted by electric current pulses.

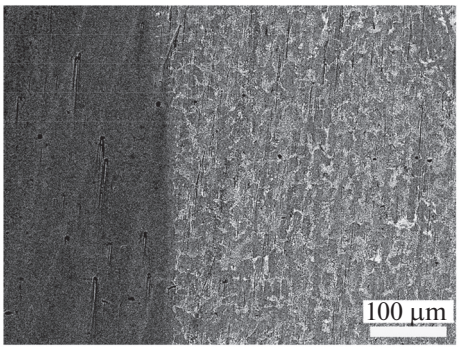

Fig. 6. Structure of the molten Ni–Si–B (70 wt %) + $MoSi_2$ (30 wt %) coating.

with carbide inclusions was detected in the coating. The boundary between the coating and the base can be seen in the peripheral regions of the melted zone, which was recorded in images with the composite contrast due to the probable segregation of boron.

In the central part of the sample, the temperature is higher and the temperature field is more homogeneous. The coating is formed by a multicomponent eutectic with inclusions of hard alloy grains, the size of which can reach 40 μm (Fig. 5). No boron precipitates along the grain boundaries and no visible signs of boron diffusion into the base were observed on the cross cut sections, which confirms the predominance of transient (0.1 s) thermal effects during the formation of composite silicon-containing coatings based on the Ni–Cr–Si–B system with solid additives.

The introduction of molybdenum disilicide (up to 30–50%) as a solid additive to the ternary composition of nickel, silicon, and boron improved the quality of the coating, namely, reduced the porosity and improved the compactness and continuity of the boundary with the base in the case of using steel and molybdenum as substrates (Fig. 6).

Molybdenum disilicide particles are well wetted with the eutectic melt and partially dissolved in it. The Vickers hardness of the dispersed disilicide reinforcing inclusions is about 1200 kgf/mm^2, and the microhardness of individual small grains reaches 2000–2600 kgf/mm^2 due to the formation of borides and molybdenum carboborides.

The surface mechanical characteristics (hardness, microhardness) are a qualitative criterion for wear resistance of coatings during abrasive wear, including the case of simultaneous thermal exposure.

Increasing the hardness by a factor of 1.5 with respect to that of the base metal can lead to an increase in the wear resistance of the coating by a factor of 2 to 10. This approach gives a completely correct estimate that is confirmed experimentally. The correct ratio of the volumes of solid inclusions and plastic matrix, the size of solid inclusions, the toughness of inclusion materials, the wetting of solid inclusions with melt of the matrix, and the minimum number of defects lead to improved wear resistance characteristics.

CONCLUSIONS

Thermal conductivity studies with variation of the porosity of consolidated disilicide materials in the range from 2% to 60% have shown that the thermal conductivity is relatively low and slightly depends on the porosity value in the case of porosities greater than 10%. A noticeable increase in the thermal conductivity was observed in dense samples with a porosity of less than 3%. The optimum consolidation temperature is 1300–1500°C. An increase of the temperature is impractical, because it does not increase the density of the samples and does not change the thermal conductivity. To ensure better mechanical properties, hot-press consolidation is preferable over sintering. At the same porosity, the thermal conductivity of the samples obtained by hot pressing is higher.

The developed technology of preparation of carbide and multicomponent powders from scrap of hard alloys and tungsten anhydride in the laboratory conditions can be used for the formation of eutectic coatings. The temperature–time parameters of the process of preparation of powders with the required chemical composition are determined. In the case of introduction of boron and silicon additives into these powders in quantities corresponding to the eutectic compositions, it is possible to obtain compositions with a melting point adjustable in the range of 1000–1200°C.

Slurry mixtures are prepared on the basis of powders of the Ni–Si–B and Ni–Cr–Si–B compositions with reinforcing additives from industrially and laboratory synthesized refractory silicides and carbides, and eutectic coatings with solid component and plastic matrix microhardnesses of 11–15 GPa are obtained by melting of them. Varying the duration of heating and the thickness of the slurry, one can control the macro- and microstructural characteristics of the composite.

Comparison of the structural characteristics and properties of the coatings has shown that rapid formation of coatings by melting allows one to obtain a protective layer of the required thickness and prevents excessive embrittlement of the base due to the formation of boride phases.

It is established that the addition of molybdenum disilicide in an amount of up to 50% increases the homogeneity of the coating without reducing its hardness. The coating is characterized by high corrosion resistance up to a temperature of about 1000°C.

CONFLICT OF INTEREST

The authors declare that they have no conflicts of interest.

REFERENCES

1. Fedorchenko, I.M., Frantsevich, I.N., and Radomysel'skii, I.D., *Poroshkovaya metallurgiya. Materialy, tekhnologiya, svoistva, oblasti primeneniya* (Powder Metallurgy: Materials, Technology, Properties, Field of Application), Kiev: Naukova Dumka, 1985.
2. Gevorkyan, E., Mamalis, A., Vovk, R., Semiatkowski, Z., Morozow, D., Nerubatskyi, V., and Morozova, O.M., Special features of manufacturing cutting inserts from nanocomposite material Al_2O_3–SiC, *J. Instrum.*, 2021, vol. 16, no. 10, art. 10015.
3. Gevorkyan, E.S., Timofeeva, L.A., Nerubats'kii, V.P., and Mel'nik, O.M., *Integrated Materials Processing Technologies: a Textbook*, Kharkiv: Ukrainian State Univ. of Railway Transport, 2016.
4. Yao, Z., Stiglich, J., and Sudarshan, T.S., Molybdenum silicide based materials and their properties, *J. Mater. Eng. Perform.*, 1999, vol. 8., no. 3, pp. 291—304.
5. Gevorkyan, E., Nerubatskyi, V., Gutsalenko, Yu., Melnik, O., and Voloshyna, L., Examination of patterns in obtaining porous structures from submicron aluminum oxide powder and its mixtures, *East.-Eur. J. Enterp. Technol.*, 2020, vol. 6, no. 6 (108), pp. 41—49.
6. Sastry, S.M., Suryanarayanan, R., and Jerina, K.L., Consolidation and mechanical properties of $MoSi_2$-based materials, *Mater. Sci. Eng. A*, 1995, vol. 192/193, pp. 881—890.
7. Gevorkyan, E.S., Nerubatskyi, V.P., Gutsalenko, Yu.H., and Morozova, O.M., Some features of ceramic foam filters energy efficient technologies development, *Modern Eng. Innovat. Technol.*, 2020, no. 14, pp. 46—60.
8. Fathi, H., Historical introduction to refractory metals, *Miner. Process. Extr. Metall. Rev.*, 2001, vol. 22, no. 1, pp. 25—53.
9. Petrovic, J.J., Toughening strategies for $MoSi_2$-based high temperature structural silicides, *Intermetallics*, 2000, vol. 8, pp. 1175—1182.
10. Gevorkyan, E., Nerubatskyi, V., Chyshkala, V., and Morozova, O., Revealing specific features of structure formation in composites based on nanopowders of synthesized zirconium dioxide, *East.-Eur. J. Enterp. Technol.*, 2021, vol. 5, no. 12 (113), pp. 6—19.

11. Gevorkyan, E.S., Nerubatskyi, V.P., Chyshkala, V.O., and Morozova, O.M., Cutting composite material based on nanopowders of aluminum oxide and tungsten monocarbide, *Modern Eng. Innovat. Technol.*, 2021, no. 15, pp. 6—14.

12. Trentler, T.J., Suryanarayanan, R., Sastry, S.M., and Buhro, W.E., Sonochemical synthesis of nanocrystalline molybdenum disilicide ($MoSi_2$), *Mater. Sci. Eng. A*, 1995, vol. 204, pp. 193—196.

13. Gaffet, E., and Malhhouroux-Gaffet, N., Nanocrystalline $MoSi_2$ phase formation induced by mechanically activated annealing, *J. Alloys Compd.*, 1994, vol. 205, pp. 27—34.

14. Gevorkyan, E., Rucki, M., Krzysiak, Z., Chishkala, V., Zurowski, W., Kucharczyk, W., Barsamyan, V., Nerubatskyi, V., Mazur, T., Morozow, D., Siemiatkowski, Z., and Caban, J., Analysis of the electroconsolidation process of fine-dispersed structures out of hot pressed Al_2O_3-WC nanopowders, *Materials*, 2021, vol. 14, no. 21, art. 6503.

15. Al'tman, V.A., Valakina, V.M., and Gluskin, Ya.A., Powder composite materials, *Poroshk. Metall.* (Kiev), 1980, no. 3, pp. 24—26.

16. Ositinskaya, G.D., and Podoba, A.P., Application of the heat flow contraction method to determine the thermal conductivity coefficient of solid bodies, *Prom. Teplotekh.,* 1981, vol. 3, no. 1, pp. 43—48.

17. Shmegera, R.S., Podoba, Ya.O., Kushch, V.I., and Belyaev, A.S., Effect of the contact conductivity of the diamond–metal binder interface on the thermal conductivity of diamond-containing composites, *J. Superhard Mater.*, 2015, vol. 37, no. 4, pp. 242—252.

18. Petrovic, J.J., Toughening strategies for $MoSi_2$-based high temperature structural silicides, *Intermetallics*, 2000, no. 8, pp. 1175–1182.

19. Litovchenko, S.V., Beresnev, V.I., Chishkala, V.A., and Manucharyan, I.A., Formation of eutectic composite coatings by high-speed melting, *Fiz. Inzh. Poverkhn.*, 2014, vol. 12, no. 1, pp. 129—139.

20. Freïk, D.M., Mikhail'onka, R.Ya., and Klanichka, V.M., *Fiz. Khim. Tverd. Tela*, 2004, vol. 5, no. 1, pp. 173—191.

21. Galushchak, M.O., Ral'chenko, V.G., Tkachuk, A.I., and Freïk, D.M., *Fiz. Khim. Tverd. Tela*, 2013, vol. 14, no. 2, pp. 317—344.

22. *Concise Encyclopedia of Composite Materials*, Kelly, A., Ed., Oxford: Pergamon Press, 1994.

23. Kim, K.J., Montoya, B., Razani, A., and Lee, K.-H., Metal hydride compacts of improved thermal conductivity, *Int. J. Hydrogen Energy*, 2001, vol. 26, pp. 609—613.

24. Gevorkyan, E.S., Nerubatskyi, V.P., Chyshkala, V.O., and Morozova, O.M., Aluminum oxide nanopowders sintering at hot pressing using direct current, *Modern Sci. Res.*, 2020, no. 14, pp. 12—18.

25. Gevorkyan, E.S., Rucki, M., Kagramanyan, A.A., and Nerubatskiy, V.P., Composite material for instrumental applications based on micro powder Al_2O_3 with additives nano-powder SiC, *Int. J. Refract. Met. Hard Mater.*, 2019, vol. 82, pp. 336–339.

26. Strong, A.B., *Fundamentals of Composites Manufacturing: Materials, Methods and Applications*, Dearborn, Mi.: Society of Manufacturing Engineers, 2008.

27. Knotek, O., and Lugsheider, E., Brazing filler metals based on reacting Ni-Cr-B-Si alloys, *Weld. J. Suppl.*, 1976, pp. 314–318.

28. Pogrebnjak, A.D., and Beresnev, V.M., *Nanocoatings, Nanosystems, Nanotechnologies*, Bentham Science Publishers, 2012.

29. Azarenkov, M.O., Beresnev, V.M., and Litovchenko, S.V., *Functional Materials and Coatings: a Tutorial*, Kharkiv: Karazin Kharkiv National Univ., 2013.

30. Gevorkyan, E.S., Morozova, O.M., Sofronov, D.S., Chyshkala, V.A., and Nerubatskyi, V.P., Composite material based on synthesized zirconium oxide nanopowders with enhanced mechanical properties, *International Workshop for Young Scientists (ISMA–2021). "Functional Materials for Technical and Biomedical Applications"*, Kharkiv, 2021, p. 29.

31. Celko, L., Klakurkova, L., Smetana, B., Slamecka, K., Zaludova, M., Hui, D., and Svejcar, J., Application of sacrificial coatings and effect of composition on Al–Al_3Ni ultrafine eutectic formation, *J. Min. Metall.*, 2014, vol. 50, pp. 31–36.

32. Pashechko, M., Lenik, K., Szulzyk-Cieplak, J., and Duda, A., Powder eutectic materials of Fe-Mn-C-B system for coatings of increased abrasive wear, in *Powder Metallurgy - Fundamentals and Case Studies*, 2017.

33. Gevorkyan, E.S., Morozova, O.M., Sofronov, D.S., Nerubatskyi, V.P., and Ponomarenko, N.S., The formation of ZrO_2–Y_2O_3-nanoparticles from fluoride solutions, *Abstracts of the* II International Advanced Study Conference on Condensed Matter and Low Temperature Physics 2021 "CM&LTP 2021", Kharkiv, 2021, p. 190.

34. Pashechko, M.I., Golubets, V.M., and Chernets, M.V., *Formirovanie i friktsionnaya stoikost' evtekticheskikh pokrytii* (Formation and Friction Stability of Eutectic Coatings), Kiev: Naukova Dumka, 1993.

35. Chishkala, V.A., Litovchenko, S.V., and Nechiporenko, E.P., Use of eutectic compositions for creation of wear-resistant coatings, *Vopr. At. Nauki Tekh.*, 2002, no. 1, pp. 175—177.
36. Gevorkyan, E., Rucki, M., Salacinski, T., Siemiatkowski, Z., Nerubatskyi, V., Kucharczyk, W., Chrzanowski, Ja., Gutsalenko, Yu., and Nejman, M., Feasibility of cobalt-free nanostructured WC cutting inserts for machining of a TiC/Fe composite, *Materials*, 2021, vol. 14, no. 12.
37. Cherepin, V.T., and Vasil'ev, M.A., *Metody i pribory dlya analiza poverkhnosti materialov* (Methods and Devices for the Analysis of the Surface of Materials), Kiev: Naukova Dumka, 1982.
38. Hemmatia, I., Raoa, J.C., and Ocelika, V., Electron microscopy characterization of Ni-Cr-B–Si–C laser deposited coatings, *Microsc. Microanal.*, 2013, vol. 19, no. 1, pp. 120–131.

Translated by O. Kadkin

SPELL: 1. OK